Assessment of ice cloud modeling capabilities for the irregularly shaped Voronoi models in climate simulations with CAM5

Ming Li[1], Husi Letu[1], Yiran Peng[3], Hiroshi Ishimoto[4], Yanluan Lin[3], Takashi Y. Nakajima[2], Anthony Baran[5,6], Zengyuan Guo[3,7], Yonghui Lei[2], Jiancheng Shi[8]

[1]Aerospace Information Research Institute, Chinese Academy of Sciences, Beijing 100010, China
[2]Research and Information Center (TRIC), Tokai University, 4-1-1 Kitakaname Hiratsuka, Kanagawa 259-1292, Japan
[3]Ministry of Education Key Laboratory for Earth System Modeling, Department of Earth System Science, Tsinghua University, Beijing 10084, China
[4]Meteorological Research Institute, Japan Meteorological Agency (JMA), Nagamine 1-1, Tsukuba 305-0052, Japan
[5]Met Office, Fitzroy Road, Exeter EX1 3PB, UK
[6]School of Physics, Astronomy and Mathematics, University of Hertfordshire, Hatfield, AL10 9AB, UK
[7]National Climate Center, China Meteorological Administration, Beijing 100081, China
[8]National Space Science Center, Chinese Academy of Sciences, Beijing 100190, China

Correspondence to: Husi Letu (husiletu@radi.ac.cn)

Abstract.

Climate models and satellite remote sensing applications require accurate descriptions of ice cloud optical and radiative properties through parameterization of their scattering properties. While abundant irregularly shaped ice particle habits present a challenge for modelling ice clouds. An irregularly shaped ice particle habit (Voronoi model) has been developed and recently suggested to be effective in inferring the microphysical and radiative properties of ice clouds from Himawari-8 and GCOM-C satellite measurements. As a continuation of previous work by Letu et al. (2016), in this study, we develop a broadband ice cloud scheme based on the Voronoi model through parameterization for use in the Community Atmosphere Model, Version 5 (CAM5). With single scattering properties of Voronoi model, ice cloud bulk scattering properties are integrate over particle size distributions of 11 field campaigns and are parameterized over particle effective diameter. The new ice cloud scheme is compared with four ice cloud schemes (the Yi, Mitchell, Baum-yang and Fu scheme), and is evaluated through the General circulation model version of the Rapid Radiative Transfer Model (RRTMG), and simulations of the top of atmosphere (TOA) shortwave and longwave cloud forcing (SWCF and LWCF) in CAM5. The Clouds and the Earth's Radiant Energy System (CERES) satellite data was selected as validation data. Results indicated that the Voronoi scheme can minimize differences between the satellite-based measurements and CAM5 simulations of global TOA SWCF compared to other four schemes, but performance is not significant for TOA LWCF. For tropical ice clouds, Voronoi scheme

30   has advantages of ice cloud modelling capabilities for shortwave (SW) and longwave (LW) spectrum over other four

schemes. In general, it is found that the Voronoi model has advantages over conventional ice cloud schemes and is sufficient

for ice cloud modelling in climate simulations with CAM5.

1 Introduction

The role of ice clouds is very important for Earth-atmosphere energy balance determination through parameterization in

35   remote sensing applications and climate models. A number of field observations, such as the First International Satellite

Cloud Climatology Project (ISCCP) Regional Experiment (FIRE-I) from October-November 1986, have shown that ice

clouds contain a large variety of particle habits, sizes and complexities (Liou, 1992), as also shown by the following

observational studies (Heymsfield et al., 2017; Yang et al., 2018; Lawson et al., 2019). Substantial studies have shown that

ice cloud parameterization scheme uncertainties are mainly related to ice particle habits, sizes and microphysical properties,

40   which can lead to substantial radiative discrepancies between satellite measurements and climate model simulations (Zhang

et al., 2005). Optimal choice of representative ice particle habit is still difficult to determine.

The single-scattering properties of the ice particle models and ice cloud parameterization are important for remote sensing

applications and climate model simulations of ice cloud radiative properties. The ice cloud parameterization accuracy is

mainly determined by the single-scattering properties of the ice particle models. Furthermore, the single-scattering properties

45   of the ice particle model mainly depend on the assumption of ice particle habits and the light-scattering numerical calculation

methods. Early studies assumed ice particles to be spherical models, and their single-scattering properties can be accurately

determined by the Lorenz-Mie theory (Hulst, 1957). These models were found to be inadequate approximations for the

treatment of ice clouds because many aircraft observation measurements have shown that ice clouds are mainly composed of

the nonspherical ice particles (Macke et al., 1996; Heymsfield et al., 2002; Heymsfield et al., 2013). In the last few decades,

50   a series of light-scattering computational methods have been developed, including the conventional geometric-optics method

(CGOM) (Cai and Liou, 1982), the improved geometric-optics method (IGOM) (Yang and Liou, 1995, 1996a; Bi et al.,

2011), the finite-difference time domain (FDTD) method (Yang and Liou, 1996b), pseudo-spectral time domain (PSTD)

method (Liu, 1997; Chen et al., 2008), discrete dipole-approximation (DDA) method (Draine and Flatau, 1994; Yurkin and

Hoekstra, 2007), the T-matrix method (Macke et al., 1995; Havemann and Baran, 2001) along with the invariant imbedding T-matrix (II-TM) method (Bi et al., 2013a; Bi et al., 2013b; Bi and Yang, 2014), and the boundary element method has been more recently applied to complex ice particle shapes without approximating the geometry of the particle (Groth et al., 2015). With these computational techniques, the research community has made significant progress towards calculating single-scattering properties (namely, the extinction efficiency, asymmetry factor, single-scattering albedo, and complete phase matrix) of nonspherical ice particles. For example, the single-scattering properties of seven ice particle habits at wavelengths from 3 to 100 μm have been computed (Yang et al., 2005) using FDTD (Yang and Liou, 1996b; Sun et al., 1999) and IGOM (Yang and Liou, 1996a). The disadvantages of the data libraries developed by (Yang et al., 2005) are several inconsistencies in the spectral region caused by differences of particle habits and computational methodologies. A spectrally consistent database including 11 ice particle habits at wavelengths from 0.2 to 100 μm, were published by (Yang et al., 2013) based on a composite method of the Amsterdam discrete dipole approximation (ADDA) (Yurkin and Hoekstra, 2007, 2011), the T-matrix (Yang et al., 2007; Bi et al., 2013a, 2013b) and the IGOM method including the edge effect (Baran and Havemann, 1999). Furthermore, features including air bubbles or aerosol, various habit ensembles, and surface roughness were added into ice particles. For example, randomly oriented hexagonal ice particles containing spherical air bubbles (inhomogeneous hexagonal monocrystals) (IHMs) (Labonnote et al., 2001) were developed for use in the ice cloud parameter retrievals from the French satellite Polarization and Directionality of the Earth's Reflectances (POLDER) measurements (Deschamps et al., 1994). An ensemble ice particle model made of hexagonal column ice particles, was developed by (Baran and Labonnote, 2007; Baran et al., 2014b) for cirrus.

With the developments of light scattering computations, increasing ice cloud parameterization schemes have been developed for ice cloud remote sensing application and climate model simulations based on above ice scattering models. Fu (1996) established an ice cloud parameterization (named Fu hereafter) based on the hexagonal ice particle to the four-stream approximation of the Fu-Liou radiative transfer models (Fu et al., 1998; Fu, 2007). Baum et al. (2005b) form a new parameterization scheme (named Baum-yang hereafter) based on nine ice particle habits from a library of Yang et al. (2013) and applied it to the development of ice cloud products in MODIS Collection 5. Yi et al. (2013) developed a parameterization (named Yi hereafter) based on a general habit mixture model that includes nine pristine habits of varying

roughness (Yang et al., 2013). Baran et al. (2014a) presented a new coupled cloud physics-radiation parameterization and

80 implemented it into the Met Office Unified Model Global Atmosphere 5.0 (GA5) configuration based on the optical

properties developed by (Baran et al., 2014b). Baran et al. (2016) developed an improved ice cloud optical property

parameterization between the model prognostic variable ice water content (IWC) and the environmental temperature. This

parameterization is now implemented in the Met Office's latest Earth System model, which is described in (Walters et al.,

2019). In the Community Earth System Model version 1.2.1 (CESM1.2.1) developed by the USA National Center for

85 Atmospheric Research (NCAR) (Hurrell et al., 2013), the atmosphere component model is the Community Atmospheric

Model version 5 (CAM5) (Neale et al., 2010). In CAM5, the ice cloud parameterization scheme developed by (Mitchell et al.,

1996a; Mitchell et al., 1996b) (named Mitchell hereafter) is utilized for ice cloud optical and radiative properties. Habits of

ice particles used for the Mitchell scheme are hexagonal, irregular ice particles, quasi-spherical and 3-D bullet rosettes

calculated from the modified anomalous diffraction approximation (MADA) (Mitchell et al., 2006). Based on CESM1.2.1

90 (Hurrell et al., 2013), the Community Integrated Earth System Model (CIESM) was developed by Tsinghua University (Lin

Y L, 2020). CAM5 in CIESM was modified with several new schemes, but it still uses the Mitchell scheme for ice cloud

properties. Different ice cloud parameterization can result in significant differences in radiative properties. Ice particle habits

is one of the most important influencing factors of ice cloud radiative properties. Zhao et al. (2018) compared three ice cloud

parameterizations in CAM5, and results showed that the difference of downward longwave flux can cause the changes of

95 overall temperature by around 3℃. Yi et al. (2013) found that the effects of ice particle surface roughness on the global

shortwave (SW) and longwave (LW) cloud radiative effects (CRE) can reach 1-2 W/m^2 and 0.37 W/m^2, respectively.

The optimal choice of ice particle habit is needed to develop the ice cloud parameterization scheme as accurately as possible

and is also significant for cloud-aerosol interactions (Liu et al., 2019; Yan and Wang, 2020). Microphysical measurements

showed that a high proportion of irregularly shaped ice particles generated in convective clouds due to collision and

100 aggregation process (Heymsfield et al., 2002). An irregularly shaped Voronoi model was developed by (Ishimoto et al., 2012)

based upon in situ microphysical measurements. Letu et al. (2016) compared five representative ice particle models using the

spherical albedo difference (SAD) method, and the results indicated that the irregularly shaped Voronoi model has

advantages over the conventional general habitat mixture (GHM) (Baum et al., 2011), IHM (Labonnote et al., 2001), 5-plate

aggregate (Baum et al., 2005a; Baum et al., 2011), apart from the ensemble ice particle model (Baran and Labonnote, 2007), which gave similar results to the Voronoi model. To date, Voronoi model has been adopted in remote sensing studies of official ice cloud products for the Second Generation Global Imager (SGLI)/Global Change Observation Mission-Climate (GCOM-C) (Letu et al., 2012; Letu et al., 2016; Nakajima et al., 2019), the AHI/Himawari-8 (Letu et al., 2018) and Multi-Spectral Imager (MSI)/Earth Cloud Aerosol and Radiation Explorer (EarthCARE) satellite programs (Illingworth et al., 2015), which will be launched in 2023 and has proven to be efficient in the remote sensing retrieval of ice cloud products (Letu et al., 2020). To build on the work of (Letu et al., 2016), this study aims to develop an ice cloud parameterization scheme (named Voronoi hereafter) based on the single-scattering properties of the Voronoi model and evaluate it through AGCM simulations of the CIESM. This study focuses on reducing uncertainties in ice cloud radiative properties and studies the influence of irregularly shaped ice particle habits on cloud radiative properties.

The current work is presented as follows. Sections 2 and 3 introduce the data and methodology used in this study. Section 4 demonstrates the influence of the Voronoi model on the cloud radiative properties through radiative transfer model and AGCM multiyear simulations. Section 5 presents the summary and conclusion of this study.

2 Single-scattering properties of the Voronoi model database

In this study, the single-scattering properties of the Voronoi model, developed by (Ishimoto et al., 2012; Letu et al., 2016), are utilized in the ice cloud parameterization. The wavelength range is from 0.2 μm to 15 μm, and the particle maximum dimensions (L) of ice particles ranges from approximately 0.5 μm to 716 μm. The single-scattering properties utilized in this study mainly include the extinction efficiency (Q_{ext}), single-scattering albedo (SSA), absorption efficiency (Q_a), asymmetry factor (g) and the scattering phase function. The refractive indices of this ice crystal habit are derived from the newest library provided by (Warren and Brandt, 2008). The database of single-scattering properties were calculated using a composite approach combining FDTD, geometric optics integral equation (GOIE) (Yang and Liou, 1996a) and GOM methods (Macke et al., 1996). Figure 1 shows the single-scattering properties of ice particles that vary with different size parameters ($SZPs$) at a fixed wavelength of 0.64 μm (Figure 1 a1-a3) and 2.21 μm (Figure 1 b1-b3), respectively. The SZP is positively correlated with L and negatively correlated with wavelength, which is shown by equation (1). Note that the FDTD and GOIE methods

are used for small (SZP < 40) and moderate particles (SZP < 300), and the GOM method is used for larger particles (SZP > 300). By treating well particle edge effects (Ishimoto et al., 2012), scattering efficiency calculated by a combination of

130   FDTD, GOIE and GOM method is coherent. The extinction efficiency at both wavelengths of 0.64 μm (Figure 1 a1) and 2.21 μm (Figure 1 b1) has a peak value when the *SZP* is equal to 10 and tends to be a constant value of 2 with an increasing *SZP* larger than 100. The minimum extinction efficiency tends to 0 with a decreasing *SZP* smaller than 10 at a wavelength of 2.21μm. The scattering efficiency at both wavelengths of 0.64 μm (Figure 1 a2) and 2.21 μm (Figure 1 b2) is strong, and thus, the absorption efficiency is weak, which is related to the imaginary value in the refractive index. The asymmetry factor

135   tends to decrease with increasing *SZP* at a wavelength of 0.64μm (Figure 1 a3). At a wavelength of 2.21μm (Figure 1 b3), there is an increasing asymmetry factor for the *SZP*s smaller than 10 and larger than 300, leading to an increasing proportion of forward scattering.

$$SZP = \frac{\pi L}{\lambda},$$ (1)

3 Methodology

140   The main flowchart of this study is described in Figure 2. Aircraft field campaigns from (Heymsfield et al., 2013) are used to determine particle size distributions (PSDs) in the form of the gamma distribution (Mitchell et al., 1996a) (see equation (2)). Based on the single-scattering properties of the Voronoi model and PSDs, the effective diameter (D_e) (see equation (7)) and the spectral bulk scattering properties of ice clouds, including spectral mass-averaged extinction coefficients (m²/g) ($K_{ext}(\lambda)$) (see equation (8)), spectral single-scattering albedo ($\varpi(\lambda)$) (see equation (9)) and spectral asymmetry factor

145   ($g(\lambda)$) (see equation (10)) are calculated for all PSDs. Then, band-averaged bulk scattering properties (see equation (11-13)) are integrated over band intervals appropriate in the General circulation model version of the Rapid Radiative Transfer Model (RRTMG) (Clough et al., 2005; Morcrette et al., 2008) and CAM5. For the SW bands, the solar constant is utilized from the solar spectrum (($S(\lambda)$) provided by (Chance and Kurucz, 2010). For the LW bands, $S(\lambda)$ is replaced with the Planck function. Then, the coefficients of the polynomial expressions of the ice cloud bulk scattering properties as functions of D_e

150   are determined in each band to develop Voronoi scheme for SW and LW spectrum. To assess the ice cloud modeling capabilities of Voronoi scheme, four typical ice cloud schemes (Details are in section 1), including the Fu (Fu et al., 1998),

Baum-yang (Baum et al., 2005b), Yi (Yi et al., 2013) and Mitchell scheme (Mitchell et al., 1996a; Mitchell et al., 1996b), are introduced for comparisons through RRTMG and CAM5 simulations. Relevant coefficients in the fitting of extinction coefficients, single-scattering albedo and asymmetry factor for above four schemes can be found in their cited literature. The

155 Clouds and the Earth's Radiant Energy System (CERES) satellite level 3 CERES_SYN1deg_Ed4A products (name SYN1deg hereafter) (Draine and Flatau, 1994; Doelling et al., 2016) is considered to be efficient in many studies (Yi et al., 2013; Zhao et al., 2018). We utilize SYN1deg 1° monthly observed TOA fluxes to validate the cloud radiative properties simulated by five schemes from the CAM5.

3.1 Parameterization of ice cloud optical properties

160 To better understand the ice cloud modelling capabilities of the Voronoi model in the CAM5 and explain how ice clouds play a role in the climate system, it is necessary to introduce the main scattering parameters to evaluate the ice particle model through ice cloud parameterization. To describe the PSDs and calculate particle concentration per unit volume, we utilize 14408 groups of microphysical data (mainly including slope (N_0), intercept (μ), and dispersion (λ) of PSDs) derived from aircraft measurements obtained in 11 field campaigns (Heymsfield et al., 2013) to determine ice particle number density (n

165 (L)) in the form of the gamma distribution (see equation (2)), where L is the ice particle maximum dimensions defined by equation (1). Detailed descriptions can be found in (Heymsfield et al., 2013). Assume that the extinction and scattering cross section is known as $\sigma_{e,s}$, and the absorption cross section can be given by $\sigma_a = \sigma_e - \sigma_s$. The extinction, scattering and absorption coefficients can be calculated by equation (3). The single-scattering albedo and co-albedo can be defined as the ratio of the scattering and absorption coefficients to the extinction coefficient in the form of equation (4), respectively. Let

170 the phase function corresponding to a volume of ice particles be P. Thus, P (μ, φ; μ', φ') denotes the redirection of the incoming intensity defined by (μ', φ') to the outgoing intensity defined by (μ, φ). The optical depth can be defined by equation (5). In plane-parallel atmospheres, changes in the diffuse intensity penetrating from below the layer considering multiple scattering processes is given by equation (6).

$$n(L) = N_0 L^\mu e^{-\lambda L} , \tag{2}$$

175 $$\beta_{e,s,a} = \int_{L_{min}}^{L_{max}} \sigma_{e,s,a} n(L) dL , \tag{3}$$

$$\varpi = \frac{\beta_s}{\beta_e}, \text{ or } 1 - \varpi = \frac{\beta_a}{\beta_e} \tag{4}$$

$$\tau = \int_z^\infty \beta_e \, dz, \tag{5}$$

$$J(\tau; \mu; \phi) = \frac{\varpi}{4\pi} \int_0^{2\pi} \int_{-1}^1 I(\tau; \mu'; \phi') P(\mu, \phi; \mu', \phi') d\mu' d\phi'$$

$$+ \frac{\varpi}{4\pi} F_\Theta P(\mu, \phi; -\mu_0, \phi_0) e^{-\tau/\mu_0} + (1 - \varpi) B[T(\tau)], \tag{6}$$

where I indicate the total (direct plus diffuse) radiance, B indicates Planck's function associated with thermal emissions, and

180 Θ is the scattering angle. Obviously, extinction coefficients, single-scattering albedo and phase function, along with solar

zenith angle are fundamental driving parameters within the transfer of diffuse intensity. Hence, to assess the effectiveness of

the Voronoi ice particles model for application in the CAM5, it is necessary to develop polynomial expressions of the

extinction coefficients, the single-scattering albedo and the asymmetry factor as functions of the effective diameter D_e.

$$D_e = \frac{3}{2} \frac{\int_{\lambda_{min}}^{\lambda_{max}} \int_{L_{min}}^{L_{max}} V(L)n(L)dL}{\int_{\lambda_{min}}^{\lambda_{max}} \int_{L_{max}}^{L_{max}} A(L)n(L)dL}, \tag{7}$$

185 $$K_{ext}(\lambda) = \frac{\int_{L_{min}}^{L_{max}} Q_{ext}(\lambda, L)A(L)n(L)dL}{\rho_{ice} \int_{L_{min}}^{L_{max}} V(L)n(L)dL}, \tag{8}$$

$$\varpi(\lambda) = \frac{\int_{L_{min}}^{L_{max}} Q_{sca}(\lambda, L)A(L)n(L)dL}{\int_{L_{min}}^{L_{max}} Q_{ext}(\lambda, L)A(L)n(L)dL}, \tag{9}$$

$$g(\lambda) = \frac{\int_{L_{min}}^{L_{max}} g(\lambda, L)\sigma_{sca}(\lambda, L)n(L)dL}{\int_{L_{min}}^{L_{max}} \sigma_{sca}(L)n(L)dL}, \tag{10}$$

$$\widetilde{K}_{ext} = \frac{\int_{\lambda_{min}}^{\lambda_{max}} \beta_{ext}(\lambda)S(\lambda)d\lambda}{\int_{\lambda_{min}}^{\lambda_{max}} S(\lambda)d\lambda}, \tag{11}$$

$$\widetilde{\varpi} = \frac{\int_{\lambda_{min}}^{\lambda_{max}} \varpi(\lambda)S(\lambda)d\lambda}{\int_{\lambda_{min}}^{\lambda_{max}} S(\lambda)d\lambda}, \tag{12}$$

190 $$\widetilde{g} = \frac{\int_{\lambda_{min}}^{\lambda_{max}} g(\lambda)S(\lambda)d\lambda}{\int_{\lambda_{min}}^{\lambda_{max}} S(\lambda)d\lambda}, \tag{13}$$

3.2 The RRTMG and CAM5 simulations

To clarify the radiative effects resulting from five different scheme, we utilize the RRTMG to calculate the upward and downward flux of five schemes for comparisons. RRTMG has 14 bands for SW spectrum and 16 longwave bands (see Table 1). RRTMG is the optional radiative transfer model applied in CAM5. Since the wavelength range is from 0.2 μm to 15 μm
195   for Voronoi model database, ice cloud parameterization scheme remains unchanged in bands larger than 15 μm. To quantify the radiative flux differences caused by five schemes under the same conditions, we design an assuming ice cloud cases in standard tropics atmospheric profile in the RRTMG. Other detailed input parameters are shown in Table 2. The vertical resolution is 60 levels for the standard tropics. The RRTMG is run by five ice cloud schemes under the same conditions, thus relative difference of fluxes can be explained by difference among five schemes. Five schemes are implemented in the
200   CAM5 for comparison of shortwave and longwave cloud forcing (SWCF and LWCF). SWCF are defined as equation (14), LWCF is defined the same with SWCF but for LW spectrum.

$$SWCF = N(F_{cloudy} - F_{clear})\,, \tag{14}$$

where F_{cloudy} and F_{clear} are the difference between downward and upward fluxes for cloudy and clear conditions, respectively, and N is the cloud fraction. The CAM5 is run in two ways: 1) the CAM5 is run with the default Mitchell
205   scheme for ice clouds and the default water cloud scheme to obtain SWCF and LWCF for the Mitchell scheme; 2) the CAM5 is run by using the other four schemes (the Voronoi, Yi, Baum-yang and Fu scheme) in place of the Mitchell scheme, along with the default water cloud scheme. The CAM run is integrated for 11 years in one-month increments, the initial first year is used for state initialization and stabilization, and the last ten-year runs were utilized for comparisons. Horizontal and vertical resolution of CAM5 run experiment is 1.9° × 2.5° and 31 levels. The run is driven by prescribed climatological sea
210   surface temperature and sea ice fraction with an annual cycle in the year 2000. Within RRTMG and CAM5 simulations, water clouds adopt a spherical particle model, its single-scattering properties are derived from the Lorenz-Mie theory (Hulst, 1957). Since the CAM5 are unable to separate ice clouds from liquid clouds efficiently, the total SWCF/LWCF difference under the same water cloud parameterization is owing to the difference among five schemes.

4 Results and discussions

215 ### 4.1 Broadband bulk optical properties of the ice cloud

Based on the integration of the single-scattering properties of the Voronoi ice model database over the PSDs and band intervals, the broadband bulk optical properties of the Voronoi scheme (Figure 3 a1-c1) are compared with properties obtained from the Mitchell (Figure 3 a2-c2), Fu (Figure 3 a3-c3), Baum-yang (Figure 3 a4-c4) and Yi (Figure 3 a5-c5) scheme for 14 bands from and D_e from 10 to 150 μm as shown in Figure 3 and their differences in Figure 4. For five

220 schemes, it is found that the mass extinction coefficients show a negative correlation with D_e and are insensitive to wavelengths. The mass extinction coefficients exceed 0.2 m²/g for D_e smaller than 20 μm, and is close to 0 m²/g for D_e larger than 100 μm. The mass extinction coefficients of the Voronoi, Mitchell, Baum-yang and Yi scheme differ little as shown in Figure 4 A1, A3, A4, respectively, and the Fu scheme has lower mass extinction coefficients than the Voronoi scheme for D_e smaller than 20 μm, with the maximum negative difference up to -0.12m²/g as shown in Figure 4 A2. As shown in Figure 3,

225 there are low mass extinction coefficients in near-infrared bands ($3.08-3.85$ μm) due to the atmospheric window region which can lead to high transmittance. The single-scattering albedo obtained from five schemes (Figure 3 b1-b5) increases with decreasing wavelengths and is close to one in near-UV, visible and near-infrared band for all D_e. This result is related with the imaginary part of the refractive index of ice particles. Except for the Fu scheme, the single-scattering albedo obtained from the other four schemes decreases with the increases of D_e in near-infrared band. This result may be because

230 large ice particles are closer to geometric optics and have a greater proportion of absorption than small ice particles that are closer to Rayleigh scattering. As shown in Figure 4 B1-B4, the single-scattering albedo of the Voronoi scheme is slightly larger than the Fu scheme and is smaller than the other three schemes in near-infrared bands. In Figure 3, the asymmetry factor obtained from five schemes (Figure 3 c1-c5) increases with increasing wavelength for all D_e. From visible to near-infrared band, the asymmetry factor increases with the growing D_e. With the increase of particle size, there are more

235 absorption inside particles and decreasing single-scattering albedo, as well as decreasing side and backward scattering, resulting in more proportions of forward scattered energy. In Figure 4, the primary difference between the Voronoi scheme and the other four schemes lies in the asymmetry factor. Results show that the Voronoi scheme has the smallest asymmetry factor among five schemes, especially in visible and near-infrared band for D_e larger than 100 μm. This is because that the

complex shapes of the Voronoi ice model with large particle size can result in significant side and backward scattering and reducing the forward scattered energy. It is consistent with findings of (Letu et al., 2016). For wavelength larger than 3 μm, the Mitchell scheme has the largest asymmetry factor compared with other four schemes, especially for D_e smaller than 50 μm. It is in a good agreement with the results in Zhao et al., (2019). Overall, since the impacts of different size distribution assumptions on the bulk optical properties of ice cloud parameterization are negligible (Heymsfield et al., 2013; Heymsfield et al., 2017), differences of broadband bulk optical properties between five schemes are originally rooted in different habits of ice particles and their single-scattering properties.

4.2 RRTMG simulation results

After the parameterization, broadband bulk single-scattering properties are subsequently parameterized as functions of D_e and 14 bands, broadband bulk optical properties of five schemes are compared to each other and their differences have been analyzed in section 4.1. To illustrate and quantify the influence of optical properties of ice cloud on its radiative effects, an ideal experiment is designed to test response of radiative flux to five ice cloud schemes under the same assuming conditions. Broadband bulk single-scattering properties of five schemes are subsequently implemented in RRTMG to simulate radiative fluxes under prescribed ice clouds in standard tropics profiles which have a high proportion of ice cloud coverage (Massie et al., 2002; Stubenrauch et al., 2013). According to observations of (Hong and Liu, 2015), top and bottom pressure of ice cloud layer is set to 125.1 and 245.5 hPa, respectively, the D_e is set to 45 μm and ice water paths (IWP) equal to 60 g m^{-2}.

Shortwave radiative fluxes profiles of cloudy-sky for five schemes and clear-sky conditions are shown in Figure 5. Obviously, the downward direct flux of five schemes should be the same due to the same cloud optical thickness. Figure 5 a1 show that cloudy-sky increases the upward flux due to larger cloud albedo compared with clear-sky conditions. Figure 5 a3 indicate cloudy-sky decrease downward flux due to the absorption effects inside the cloud. Net flux under cloudy-sky is smaller than clear-sky (Figure 5 a4), which can explain the cooling effects of ice cloud for SW spectrum. Figure 5 a3 show that cloudy-sky increase the downward diffuse fluxes owing to multiple and single scattering. Specific comparison of five schemes inside the black dotted region of Figure 5 a1 - a2, are enlarged and shown in Figure 5 a1' - a4'. In Figure 5 a1', upward fluxes of five schemes and their differences gradually increase from cloud bottom to cloud top, reaching to the maximum at the cloud top. The Voronoi and Mitchell scheme have higher upward fluxes (Figure 5 a1') and lower downward

diffuse flux (Figure 5 a2') than the other three schemes. Differences of Voronoi scheme minus the Mitchell, Yi, Baum-yang and Fu scheme are 6-30 W/m² for TOA upward fluxes, and -10-(-40) W/m² for surface downward diffuse flux, -10- (-30) W/m2 for surface net fluxes, and -8-(-42) W/m² for TOA net fluxes. Radiative properties of Voronoi scheme in SW fluxes can be explained by its smaller asymmetry factor (Figure 3, 4) than the other four schemes, leading to smaller proportion of forward scattering and larger backward scattering. Thus, less SW flux reaching the ground and more upward flux for the Voronoi scheme compared with the other four schemes. Five schemes rank as the Voronoi, Mitchell, Yi, Baum-yang and Fu scheme for upward fluxes and the opposite rank for downward diffuse fluxes.

4.3 CAM5 simulation results

As shown in RRTMG simulations in section 4.2, the influence of five ice cloud schemes (the Voronoi, Yi, Mitchell, Baum-yang and Fu scheme) on the radiative effects is evaluated under standard tropical atmospheric profiles, and with assumptions of ice cloud microphysical properties as input data. Simulation results based upon radiative transfer model are capable of showing difference of ice cloud radiative effects for five schemes under some specific conditions, but are unable to demonstrate comprehensive performance of five schemes corresponding to real atmospheric situation. To study the ice cloud modelling capabilities of five schemes as accurately as possible, the Voronoi, Yi, Baum-yang and Fu scheme are applied in CAM5 in place of the default scheme (Mitchell scheme). Figure 6 and Figure 7 show the 10-yr mean TOA SWCF and LWCF calculated from CERES SYN1deg products, and CAM5-simulated 10-yr average TOA SWCF and LWCF for five schemes. Obviously, SWCF and LWCF exhibit cooling and warming effects, respectively. It is found that SWCF and LWCF of SYN1deg products and CAM5 simulations are strong in tropics where frequent ice and liquid clouds occur. In CAM5 simulations for five schemes, the liquid water scheme remains unchanged, hence the difference of the total TOA SWCF and LWCF among five schemes are attributed to different ice habits and their scattering and absorption properties within five schemes. On a global average (Table 3), SWCF differences of CERES SYN1deg data minus CAM5 simulations in ascending order, are the Voronoi (-0.33 W/m²), Mitchell (-1.11W/m²), Yi (-2.03W/m²), Baum-yang (-2.91 W/m²) and Fu scheme (-4.02 W/m²). LWCF differences of CERES SYN1deg data minus CAM5 simulations in ascending order, are the Voronoi (-0.39 W/m²), Mitchell (-0.76 W/m²), Baum-yang (-0.86 W/m²), Yi (-0.88 W/m²) and Fu scheme (-1.11 W/m²).

To discuss the influence of five schemes on the global distributions of SWCF and LWCF, the zonal mean analyses are shown in Figure 8. Results shows that the Voronoi scheme exhibits weaker cooling effects and weaker warming effects in

290   tropical regions than the other four schemes, and reduce the differences of TOA SWCF and LWCF between the CAM5 simulations and CERES SYN1deg products. As shown in RRTMG simulations (Figure 5), among five schemes, the Voronoi scheme has lowest SW net flux, which can obtain smallest SWCF according to equation (14). That is why the Voronoi scheme is closest to the CERES SYN1deg data over tropics region. Figure 9 show distribution of differences between five schemes minus CERES SYN1deg mean values. The differences box of Voronoi scheme are most concentrated on the zero

295   line, and its statistical deviation is the smallest, which means the spatial distribution of cloud radiative effects of Voronoi scheme is closer to CERES observed results compared with other four schemes.

5 Conclusions

This paper attempts to evaluate the influence of the irregularly shaped Voronoi model on the cloud radiative effects through parameterization (named Voronoi scheme) in the Community Atmosphere Model, Version 5 (CAM5). Bulk optical

300   properties, standalone radiative model simulations based on RRTMG and CAM5 10-yr simulation results of Voronoi scheme are compared with the Mitchell scheme (the default scheme of the CAM5) and other four schemes (the Fu, Mitchell, Baum-yang and Yi). The conclusions are as follows.

Comparisons of broadband bulk ice cloud optical property indicate that the Voronoi scheme shows similar mass extinction coefficients and single-scattering albedos compared with the other four schemes. The Voronoi scheme produces a smaller

305   asymmetry factor, which can cause stronger backward scattering, due to its complex shape. The RRTMG simulations exhibit the shortwave upward and downward flux profiles of five schemes. Results show that weaker absorption in the Voronoi scheme leads to more upward flux at the TOA but less downward flux at the surface in tropical cases, as well as reducing the warming effects below the cloud more than the Mitchell scheme. Through 10-yr CAM5 simulations, this paper analysis the feedback effects of Voronoi scheme and existing four schemes on the climate system and their differences. The globally

310   averaged TOA SWCF and LWCF induced by five ice cloud schemes produce 1.5% (6.3%), 2.2% (6.6%), 10.2% (6.4%), 9.3% (8.4%) and 6.8% (7.1%) difference against CERES, respectively.

In conclusion, Comparisons among Voronoi scheme, Baum-yang scheme, Yi scheme, Fu scheme, Mitchell scheme and CERES satellite observation show that Voronoi scheme generally agrees with satellite observations. The Voronoi model has the advantage of ice cloud modelling capabilities in CAM5 and possesses the potential for application in other global and

315   zonal climate models. Tuning the ice cloud schemes in other climate models may effectively fix the discrepancy between the simulations and observations.

Data availability

The RRTMG code are available at http://rtweb.aer.com/rrtmg_sw_code.html, the CERES level3 SYN1deg products are available at https://ceres.larc.nasa.gov/data/.

320   **Author contribution**

Husi Letu designed this research and helped guiding and reviewing the paper. Ming Li completed the experiments and wrote the initial draft of this manuscript. Yiran Peng, Yanluan Lin and ZengYuan Guo providing the climate model run platform and environment, as well as helped guiding the experiments and reviewing the paper. Anthony Baran helped reviewing and editing the paper. Yonghui Lei helped reviewing the paper.

325   **Competing interests**

The authors declare that they have no conflict of interests.

Acknowledgement

This work is supported by the Second Tibetan Plateau Scientific Expedition and Research Program (STEP) (Grant No. 2019QZKK0206), National Natural Science Foundation of China (Grant No. 42025504, 41771395) and International

330   Partnership Programme of Bureau of International Cooperation Chinese Academy of Sciences (Contract No. 181811KYSB20190014).

References

Baran, A. J., and Havemann, S.: Rapid computation of the optical properties of hexagonal columns using complex angular momentum theory, J Quant Spectrosc Ra, 63, 499-519, 1999.

335 Baran, A. J., and Labonnote, L. C.: A self-consistent scattering model for cirrus. I: The solar region, Q J Roy Meteor Soc, 133, 1899-1912, 10.1002/qj.164, 2007.

Baran, A. J., Hill, P., Furtado, K., Field, P., and Manners, J.: A Coupled Cloud Physics Radiation Parameterization of the Bulk Optical Properties of Cirrus and Its Impact on the Met Office Unified Model Global Atmosphere 5.0 Configuration, J Climate, 27, 7725-7752, 2014a.

340 Baran, A. J., Cotton, R., Furtado, K., Havemann, S., Labonnote, L. C., Marenco, F., Smith, A., and Thelen, J. C.: A self-consistent scattering model for cirrus. II: The high and low frequencies, Q J Roy Meteor Soc, 140, 1039-1057, 10.1002/qj.2193, 2014b.

Baum, B. A., Heymsfield, A. J., Yang, P., and Bedka, S. T.: Bulk scattering properties for the remote sensing of ice clouds. Part I: Microphysical data and models, J Appl Meteorol, 44, 1885-1895, 2005a.

Baum, B. A., Yang, P., Heymsfield, A. J., Platnick, S., King, M. D., Hu, Y. X., and Bedka, S. T.: Bulk scattering properties for the remote

345 sensing of ice clouds. Part II: Narrowband models, J Appl Meteorol, 44, 1896-1911, 2005b.

Baum, B. A., Yang, P., Heymsfield, A. J., Schmitt, C. G., Xie, Y., Bansemer, A., Hu, Y. X., and Zhang, Z. B.: Improvements in Shortwave Bulk Scattering and Absorption Models for the Remote Sensing of Ice Clouds, J Appl Meteorol Clim, 50, 1037-1056, 2011.

Bi, L., Yang, P., Kattawar, G. W., Hu, Y. X., and Baum, B. A.: Scattering and absorption of light by ice particles: Solution by a new physical-geometric optics hybrid method, J Quant Spectrosc Ra, 112, 1492-1508, 10.1016/j.jqsrt.2011.02.015, 2011.

350 Bi, L., Yang, P., Kattawar, G. W., and Mishchenko, M. I.: A numerical combination of extended boundary condition method and invariant imbedding method applied to light scattering by large spheroids and cylinders, J Quant Spectrosc Ra, 123, 17-22, 10.1016/j.jqsrt.2012.11.033, 2013a.

Bi, L., Yang, P., Kattawar, G. W., and Mishchenko, M. I.: Efficient implementation of the invariant imbedding T-matrix method and the separation of variables method applied to large nonspherical inhomogeneous particles, J Quant Spectrosc Ra, 116, 169-183,

355 10.1016/j.jqsrt.2012.11.014, 2013b.

Bi, L., and Yang, P.: Accurate simulation of the optical properties of atmospheric ice crystals with the invariant imbedding T-matrix method, J Quant Spectrosc Ra, 138, 17-35, 2014.

Cai, Q., and Liou, K. N.: Polarized-Light Scattering by Hexagonal Ice Crystals - Theory, Appl Optics, 21, 3569-3580, 1982.

Chance, K., and Kurucz, R. L.: An improved high-resolution solar reference spectrum for earth's atmosphere measurements in the ultraviolet, visible, and near infrared, J Quant Spectrosc Ra, 111, 1289-1295, 2010.

Chen, G., Yang, P., and Kattawar, G. W.: Application of the pseudospectral time-domain method to the scattering of light by nonspherical particles, J Opt Soc Am A, 25, 785-790, 2008.

Clough, S. A., Shephard, M. W., Mlawer, E., Delamere, J. S., Iacono, M., Cady-Pereira, K., Boukabara, S., and Brown, P. D.: Atmospheric radiative transfer modeling: a summary of the AER codes, J Quant Spectrosc Ra, 91, 233-244, 2005.

Deschamps, P. Y., Breon, F. M., Leroy, M., Podaire, A., Bricaud, A., Buriez, J. C., and Seze, G.: The Polder Mission - Instrument Characteristics and Scientific Objectives, Ieee T Geosci Remote, 32, 598-615, 1994.

Doelling, D. R., Sun, M., Nguyen, L. T., Nordeen, M. L., Haney, C. O., Keyes, D. F., and Mlynczak, P. E.: Advances in Geostationary-Derived Longwave Fluxes for the CERES Synoptic (SYN1deg) Product, J Atmos Ocean Tech, 33, 503-521, 2016.

Draine, B. T., and Flatau, P. J.: Discrete-Dipole Approximation for Scattering Calculations, J Opt Soc Am A, 11, 1491-1499, 1994.

Fu, Q., Yang, P., and Sun, W. B.: An accurate parameterization of the infrared radiative properties of cirrus clouds for climate models, J Climate, 11, 2223-2237, Doi 10.1175/1520-0442(1998)011<2223:Aapoti>2.0.Co;2, 1998.

Fu, Q.: A new parameterization of an asymmetry factor of cirrus clouds for climate models, J Atmos Sci, 64, 4140-4150, 2007.

Fu, Q. A.: An accurate parameterization of the solar radiative properties of cirrus clouds for climate models, J Climate, 9, 2058-2082, Doi 10.1175/1520-0442(1996)009<2058:Aapots>2.0.Co;2, 1996.

Groth, S. P., Baran, A. J., Betcke, T., Havemann, S., and Smigaj, W.: The boundary element method for light scattering by ice crystals and its implementation in BEM plus, J Quant Spectrosc Ra, 167, 40-52, 2015.

Havemann, S., and Baran, A. J.: Extension of T-matrix to scattering of electromagnetic plane waves by non-axisymmetric dielectric particles: application to hexagonal ice cylinders, J Quant Spectrosc Ra, 70, 139-158, 2001.

Heymsfield, A. J., Bansemer, A., Field, P. R., Durden, S. L., Stith, J. L., Dye, J. E., Hall, W., and Grainger, C. A.: Observations and parameterizations of particle size distributions in deep tropical cirrus and stratiform precipitating clouds: Results from in situ observations in TRMM field campaigns, J Atmos Sci, 59, 3457-3491, 2002.

Heymsfield, A. J., Schmitt, C., and Bansemer, A.: Ice Cloud Particle Size Distributions and Pressure-Dependent Terminal Velocities from In Situ Observations at Temperatures from 0 degrees to-86 degrees C, J Atmos Sci, 70, 4123-4154, 2013.

Heymsfield, A. J., Krämer, M., Luebke, A., Brown, P., Cziczo, D. J., Franklin, C., Lawson, P., Lohmann, U., McFarquhar, G., Ulanowski, Z., and Van Tricht, K.: Cirrus Clouds, Meteorological Monographs, 58, 2.1-2.26, 10.1175/AMSMONOGRAPHS-D-16-0010.1, 2017.

Hong, Y. L., and Liu, G. S.: The Characteristics of Ice Cloud Properties Derived from CloudSat and CALIPSO Measurements, J Climate, 28, 3880-3901, 2015.

Hulst, H. C. v. d.: Light scattering by small particles, Structure of matter series, Wiley, New York,, xiii, 470 p. pp., 1957.

Hurrell, J. W., Holland, M. M., Gent, P. R., Ghan, S., Kay, J. E., Kushner, P. J., Lamarque, J. F., Large, W. G., Lawrence, D., Lindsay, K.,
390   Lipscomb, W. H., Long, M. C., Mahowald, N., Marsh, D. R., Neale, R. B., Rasch, P., Vavrus, S., Vertenstein, M., Bader, D., Collins, W. D., Hack, J. J., Kiehl, J., and Marshall, S.: The Community Earth System Model A Framework for Collaborative Research, B Am Meteorol Soc, 94, 1339-1360, 2013.

Illingworth, A. J., Barker, H. W., Beljaars, A., Ceccaldi, M., Chepfer, H., Clerbaux, N., Cole, J., Delanoe, J., Domenech, C., Donovan, D. P., Fukuda, S., Hirakata, M., Hogan, R. J., Huenerbein, A., Kollias, P., Kubota, T., Nakajima, T., Nakajima, T. Y., Nishizawa, T.,
395   Ohno, Y., Okamoto, H., Oki, R., Sato, K., Satoh, M., Shephard, M. W., Velazquez-Blazquez, A., Wandinger, U., Wehr, T., and van Zadelhoff, G.-J.: THE EARTHCARE SATELLITE The Next Step Forward in Global Measurements of Clouds, Aerosols, Precipitation, and Radiation, B Am Meteorol Soc, 96, 1311-1332, 2015.

Ishimoto, H., Masuda, K., Mano, Y., Orikasa, N., and Uchiyama, A.: Irregularly shaped ice aggregates in optical modeling of convectively generated ice clouds, J Quant Spectrosc Ra, 113, 632-643, 2012.

400   Labonnote, L. C., Brogniez, G., Buriez, J. C., Doutriaux-Boucher, M., Gayet, J. F., and Macke, A.: Polarized light scattering by inhomogeneous hexagonal monocrystals: Validation with ADEOS-POLDER measurements, J Geophys Res-Atmos, 106, 12139-12153, 2001.

Lawson, R. P., Woods, S., Jensen, E., Erfani, E., Gurganus, C., Gallagher, M., Connolly, P., Whiteway, J., Baran, A. J., May, P., Heymsfield, A., Schmitt, C. G., McFarquhar, G., Um, J., Protat, A., Bailey, M., Lance, S., Muehlbauer, A., Stith, J., Korolev, A.,
405   Toon, O. B., and Kramer, M.: A Review of Ice Particle Shapes in Cirrus formed In Situ and in Anvils, J Geophys Res-Atmos, 124, 10049-10090, 2019.

Letu, H., Nakajima, T. Y., and Matsui, T. N.: Development of an ice crystal scattering database for the global change observation mission/second generation global imager satellite mission: investigating the refractive index grid system and potential retrieval error, Appl Optics, 51, 6172-6178, 2012.

410   Letu, H., Ishimoto, H., Riedi, J., Nakajima, T. Y., Labonnote, L. C., Baran, A. J., Nagao, T. M., and Sekiguchi, M.: Investigation of ice particle habits to be used for ice cloud remote sensing for the GCOM-C satellite mission, Atmos Chem Phys, 16, 12287-12303, 2016.

Letu, H. S., Nagao, T. M., Nakajima, T. Y., Riedi, J., Ishimoto, H., Baran, A. J., Shang, H. Z., Sekiguchi, M., and Kikuchi, M.: Ice Cloud Properties From Himawari-8/AHI Next-Generation Geostationary Satellite: Capability of the AHI to Monitor the DC Cloud Generation Process, Ieee T Geosci Remote, 57, 3229-3239, 2018.

415 Letu, H. S., Yang, K., Nakajima, T. Y., Ishimoto, H., Nagao, T. M., Riedi, J., Baran, A. J., Ma, R., Wang, T. X., Shang, H. Z., Khatri, P., Chen, L. F., Shi, C. X., and Shi, J. C.: High-resolution retrieval of cloud microphysical properties and surface solar radiation using Himawari-8/AHI next-generation geostationary satellite, Remote Sens Environ, 239, 2020.

Lin Y L, H. X. M., Liang Y S, et al.: The Community Integrated Earth System Model (CIESM) from Tsinghua University and its plan for CMIP6 experiments, Climate Change Research, 15 (5), 0, 2020.

420 Liu, Q. H.: The PSTD algorithm: A time-domain method requiring only two cells per wavelength, Microw Opt Techn Let, 15, 158-165, 1997.

Liu, Y. Z., Hua, S., Jia, R., and Huang, J. P.: Effect of Aerosols on the Ice Cloud Properties Over the Tibetan Plateau, J Geophys Res-Atmos, 124, 9594-9608, 2019.

Macke, A., Mishchenko, M. I., Muinonen, K., and Carlson, B. E.: Scattering of Light by Large Nonspherical Particles - Approximation
425 Versus T-Matrix Method, Opt Lett, 20, 1934-1936, 1995.

Macke, A., Mueller, J., and Raschke, E.: Single scattering properties of atmospheric ice crystals, J Atmos Sci, 53, 2813-2825, Doi 10.1175/1520-0469(1996)053<2813:Sspoai>2.0.Co;2, 1996.

Massie, S., Gettelman, A., Randel, W., and Baumgardner, D.: Distribution of tropical cirrus in relation to convection, J Geophys Res-Atmos, 107, 2002.

430 Mitchell, David, L., Liu, Yangang, Macke, and Andreas: Modeling Cirrus Clouds. Part II: Treatment of Radiative Properties, J. Atmos. Sci, 53, 2967-2988, 1996b.

Mitchell, D. L., Chai, S. K., Liu, Y. G., Heymsfield, A. J., and Dong, Y. Y.: Modeling Cirrus Clouds. Part I: Treatment of Bimodal Size Spectra and Case Study Analysis, J Atmos Sci, 53, 2952-2966, 1996a.

Mitchell, D. L., Baran, A. J., Arnott, W. P., and Schmitt, C.: Testing and comparing the modified anomalous diffraction approximation, J
435 Atmos Sci, 63, 2948-2962, 2006.

Morcrette, J. J., Barker, H. W., Cole, J. N. S., Iacono, M. J., and Pincus, R.: Impact of a New Radiation Package, McRad, in the ECMWF Integrated Forecasting System, Mon Weather Rev, 136, 4773-4798, 2008.

Nakajima, T. Y., Ishida, H., Nagao, T. M., Hori, M., Letu, H., Higuchi, R., Tamaru, N., Imoto, N., and Yamazaki, A.: Theoretical basis of the algorithms and early phase results of the GCOM-C (Shikisai) SGLI cloud products, Prog Earth Planet Sc, 6, 2019.

440   Neale, R. B., Gettelman, A., Park, S., Conley, A. J., Kinnison, D., Marsh, D., Smith, A. K., Vitt, F., Morrison, H., and Cameronsmith, P.:
Description of the NCAR Community Atmosphere Model (CAM 5.0), Tech. Note NCAR/TN-486+STR, Natl. Cent. for Atmos, Land
Model .ncar Tech.note Ncar, tn-486+str, 2010.

Stubenrauch, C. J., Rossow, W. B., Kinne, S., Ackerman, S., Cesana, G., Chepfer, H., Di Girolamo, L., Getzewich, B., Guignard, A.,
Heidinger, A., Maddux, B. C., Menzel, W. P., Minnis, P., Pearl, C., Platnick, S., Poulsen, C., Riedi, J., Sun-Mack, S., Walther, A.,
445   Winker, D., Zeng, S., and Zhao, G.: Assessment of Global Cloud Datasets from Satellites: Project and Database Initiated by the
GEWEX Radiation Panel, B Am Meteorol Soc, 94, 1031-1049, 2013.

Sun, W. B., Fu, Q., and Chen, Z. Z.: Finite-difference time-domain solution of light scattering by dielectric particles with a perfectly
matched layer absorbing boundary condition, Appl Optics, 38, 3141-3151, 1999.

Walters, D., Baran, A. J., Boutle, I., Brooks, M., Earnshaw, P., Edwards, J., Furtado, K., Hi, P., Lock, A., Manners, J., Morcrette, C.,
450   Mulcahy, J., Sanchez, C., Smith, C., Stratton, R., Tennant, W., Tomassini, L., Van Weverberg, K., Vosper, S., Willett, M., Browse, J.,
Bushell, A., Carslaw, K., Dalvi, M., Essery, R., Gedney, N., Hardiman, S., Johnson, B., Johnson, C., Jones, A., Jones, C., Mann, G.,
Milton, S., Rumbold, H., Sellar, A., Ujiie, M., Whitall, M., Williams, K., and Zerroukat, M.: The Met Office Unified Model Global
Atmosphere 7.0/7.1 and JULES Global Land 7.0 configurations, Geosci Model Dev, 12, 1909-1963, 2019.

Warren, S. G., and Brandt, R. E.: Optical constants of ice from the ultraviolet to the microwave: A revised compilation, J Geophys Res-
455   Atmos, 113, 2008.

Yan, H. R., and Wang, T. H.: Ten Years of Aerosol Effects on Single-Layer Overcast Clouds over the US Southern Great Plains and the
China Loess Plateau, Adv Meteorol, 2020, 2020.

Yang, P., and Liou, K. N.: Light-Scattering by Hexagonal Ice Crystals - Comparison of Finite-Difference Time-Domain and Geometric
Optics Models, J Opt Soc Am A, 12, 162-176, 1995.

460   Yang, P., and Liou, K. N.: Geometric-optics-integral-equation method for light scattering by nonspherical ice crystals, Appl Optics, 35,
6568-6584, 1996a.

Yang, P., and Liou, K. N.: Finite-difference time domain method for light scattering by small ice crystals in three-dimensional space, J Opt
Soc Am A, 13, 2072-2085, 1996b.

Yang, P., Wei, H. L., Huang, H. L., Baum, B. A., Hu, Y. X., Kattawar, G. W., Mishchenko, M. I., and Fu, Q.: Scattering and absorption
465   property database for nonspherical ice particles in the near- through far-infrared spectral region, Appl Optics, 44, 5512-5523, 2005.

Yang, P., Bi, L., Baum, B. A., Liou, K. N., Kattawar, G. W., Mishchenko, M. I., and Cole, B.: Spectrally Consistent Scattering, Absorption, and Polarization Properties of Atmospheric Ice Crystals at Wavelengths from 0.2 to 100 mu m, J Atmos Sci, 70, 330-347, 10.1175/Jas-D-12-039.1, 2013.

Yang, P., Hioki, S., Saito, M., Kuo, C. P., Baum, B. A., and Liou, K. N.: A Review of Ice Cloud Optical Property Models for Passive Satellite Remote Sensing, Atmosphere-Basel, 9, 2018.

Yi, B. Q., Yang, P., Baum, B. A., L'Ecuyer, T., Oreopoulos, L., Mlawer, E. J., Heymsfield, A. J., and Liou, K. N.: Influence of Ice Particle Surface Roughening on the Global Cloud Radiative Effect, J Atmos Sci, 70, 2794-2807, 2013.

Yurkin, M. A., and Hoekstra, A. G.: The discrete dipole approximation: An overview and recent developments, J Quant Spectrosc Ra, 106, 558-589, 2007.

Yurkin, M. A., and Hoekstra, A. G.: The discrete-dipole-approximation code ADDA: Capabilities and known limitations, J Quant Spectrosc Ra, 112, 2234-2247, 2011.

Zhang, M. H., Lin, W. Y., Klein, S. A., Bacmeister, J. T., Bony, S., Cederwall, R. T., Del Genio, A. D., Hack, J. J., Loeb, N. G., Lohmann, U., Minnis, P., Musat, I., Pincus, R., Stier, P., Suarez, M. J., Webb, M. J., Wu, J. B., Xie, S. C., Yao, M. S., and Zhang, J. H.: Comparing clouds and their seasonal variations in 10 atmospheric general circulation models with satellite measurements, J Geophys Res-Atmos, 110, Artn D15s0210.1029/2004jd005021, 2005.

Zhao, W. J., Peng, Y. R., Wang, B., Yi, B. Q., Lin, Y. L., and Li, J. N.: Comparison of three ice cloud optical schemes in climate simulations with community atmospheric model version 5, Atmos Res, 204, 37-53, 2018.

Tables:

490

Table 1. Shortwave and longwave bands in RRTMG

Shortwave		Longwave	
Band	μm	Band	cm-1
16	3.08–3.85	1	10–350
17	2.5–3.08	2	350–500
18	2.15–2.5	3	500–630
19	1.94–2.15	4	630–700
20	1.63–1.94	5	700–820
21	1.3–1.63	6	820–980
22	1.24–1.3	7	980–1080
23	0.78–1.24	8	1080–1180
24	0.63–0.78	9	1180–1390
25	0.44–0.63	10	1390–1480
26	0.34–0.44	11	1480–1800
27	0.26–0.34	12	1800–2080
28	0.2–0.26	13	2080–2250
29	3.85–12.2	14	2250–2380
		15	2380–2600
		16	2600–3250

495

500

505

510

Table 2. Input parameter settings in RRTMG

Cases	Pressure (hPa)	Ice water path (g/m²)	Ice particle effective size (μm)	Cloud fraction (%)	Solar zenith angle (°θ)	Surface albedo
High ice cloud	125.1 - 245.5	60	45	0.5	60	0.1

515

520

525

530

Table3. TOA SWCF and LWCF for five schemes and satellite observations.

	Baum-yang scheme	Fu scheme	Yi scheme	Mitchell scheme	Voronoi scheme	CERES SYN1deg
TOA SWCF	-45.55	-46.66	-44.67	-43.73	-42.97	-42.64
TOA LWCF	20.11	19.86	20.09	20.21	20.58	20.97
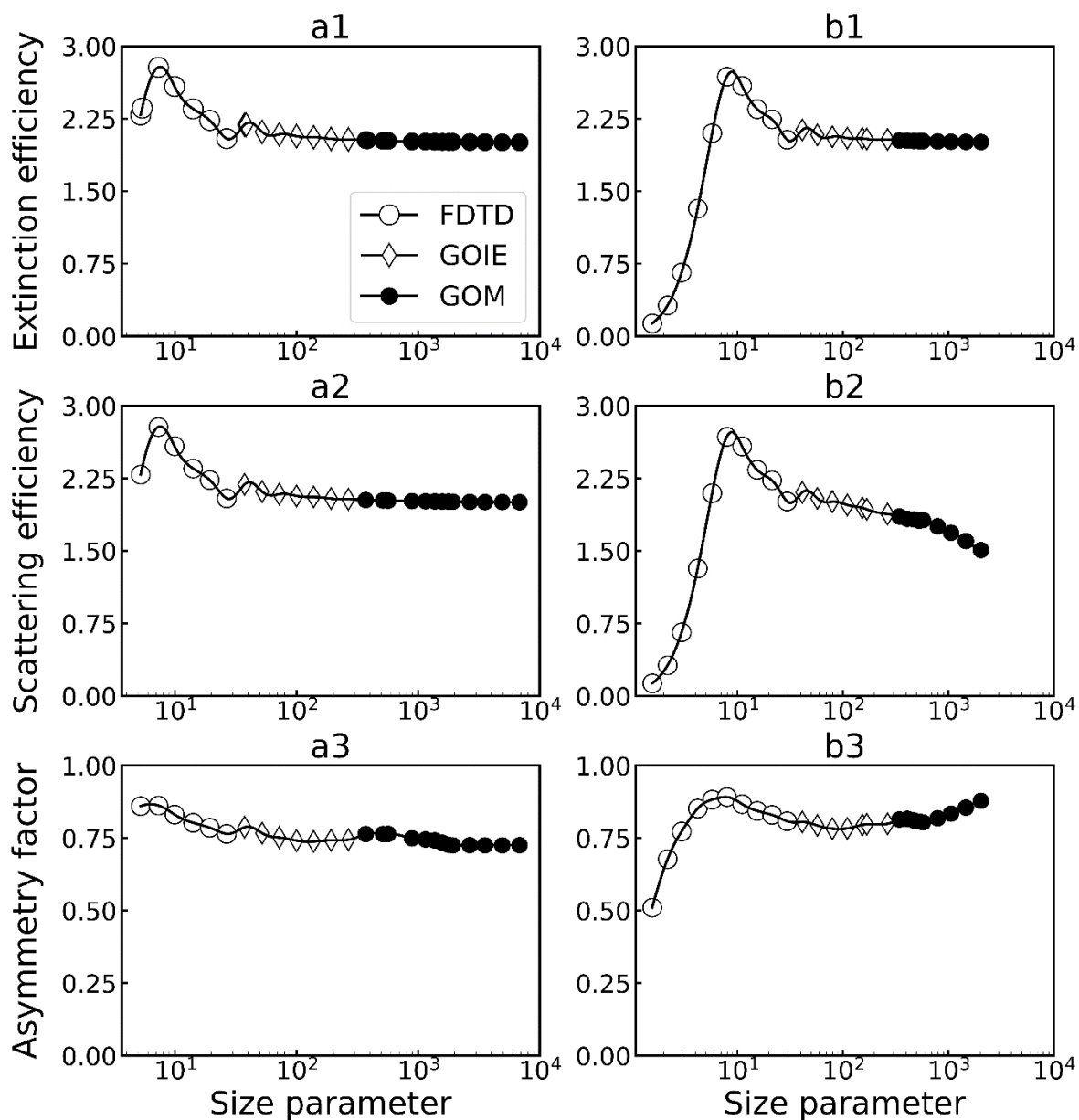
Figures:

Figure 1. Single scattering properties (extinction efficiency, scattering efficiency and asymmetry factor) of Voronoi model from the composite method based on the FDTD, GOIE, and GOM methods at fixed wavelength of (a) 0.64µm and (b) 2.21µm, respectively.
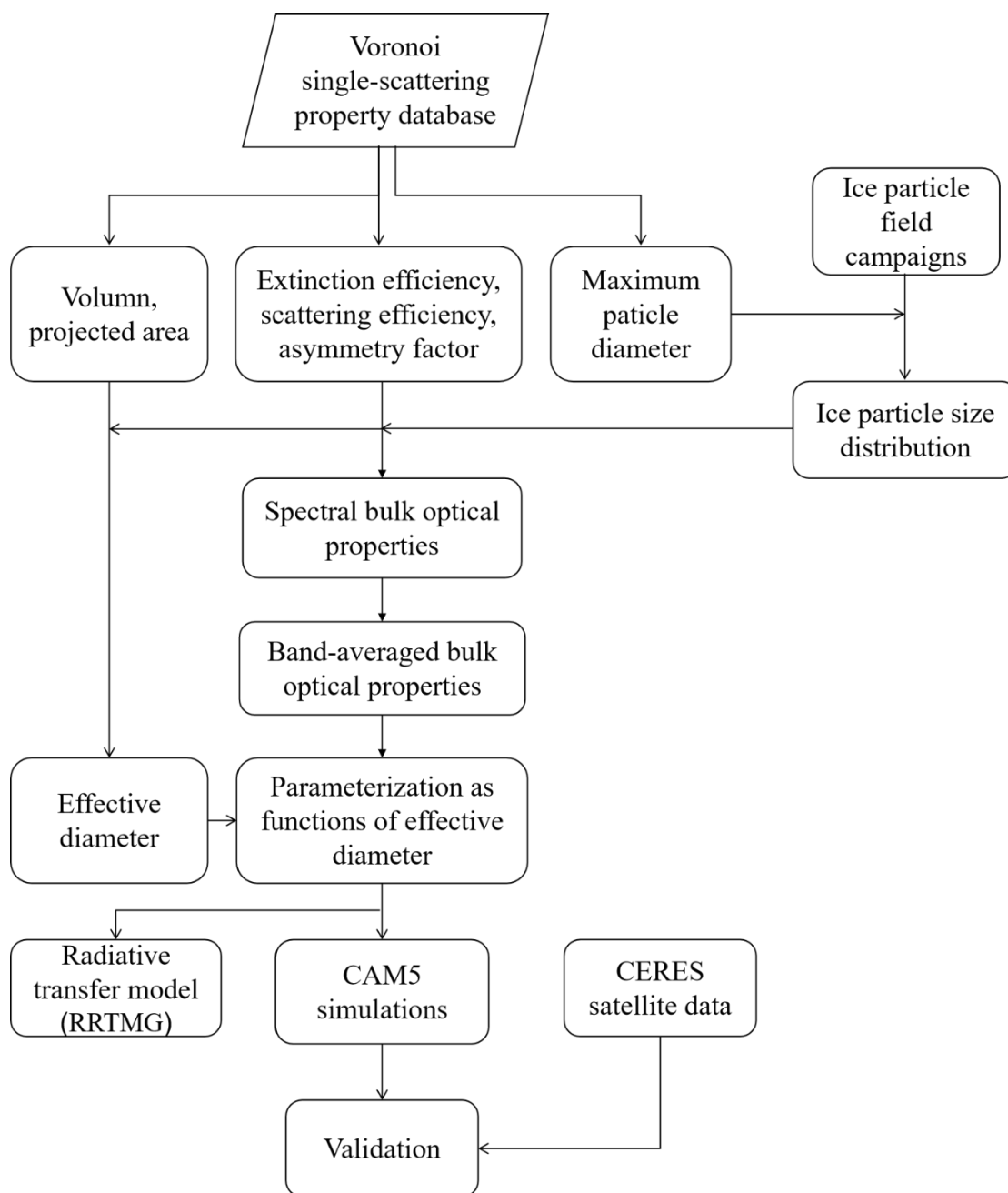
575

Figure 2. The framework of the steps of the ice cloud parameterization based on the Voronoi model.
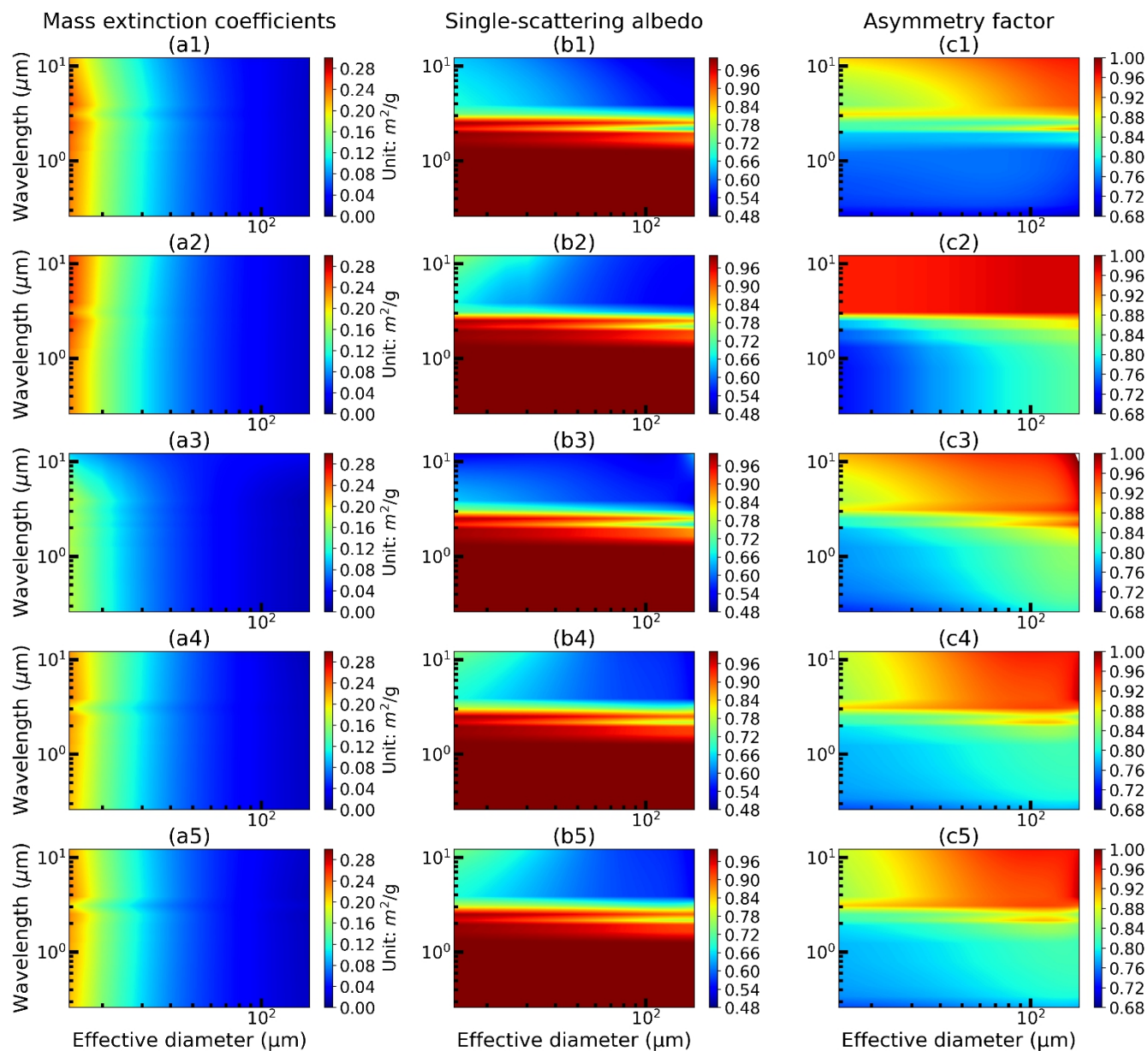
Figure 3. Calculations of (left) mass extinction coefficients, (center) single scattering albedo and (right) asymmetry factor as a function of ice particle effective diameter D_e and 14 shortwave bands for (top row) Voronoi scheme, (second row) Mitchell scheme, (third row) Fu scheme, (fourth row) Baum-yang scheme, and (bottom row) Yi scheme.
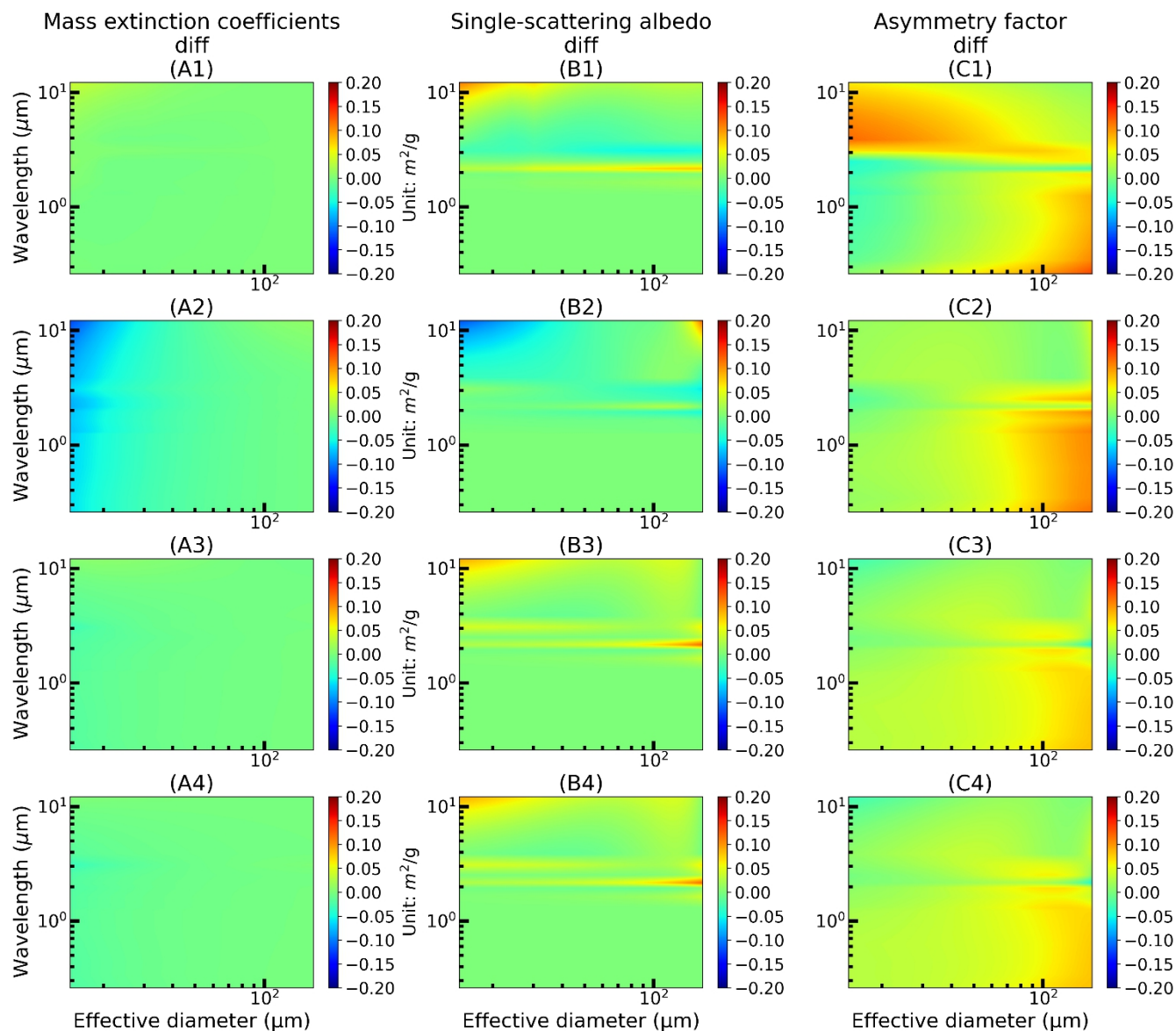
Figure 4. Differences in (left) mass extinction coefficients, (center) single scattering albedo and (right) asymmetry factor as a function of ice particle effective diameter D_e and 14 shortwave bands for (top row) Mitchell minus Voronoi scheme, (second row) Fu minus Voronoi scheme, (third row) Baum-yang minus Voronoi scheme, and (bottom row) Yi minus Voronoi scheme.

585
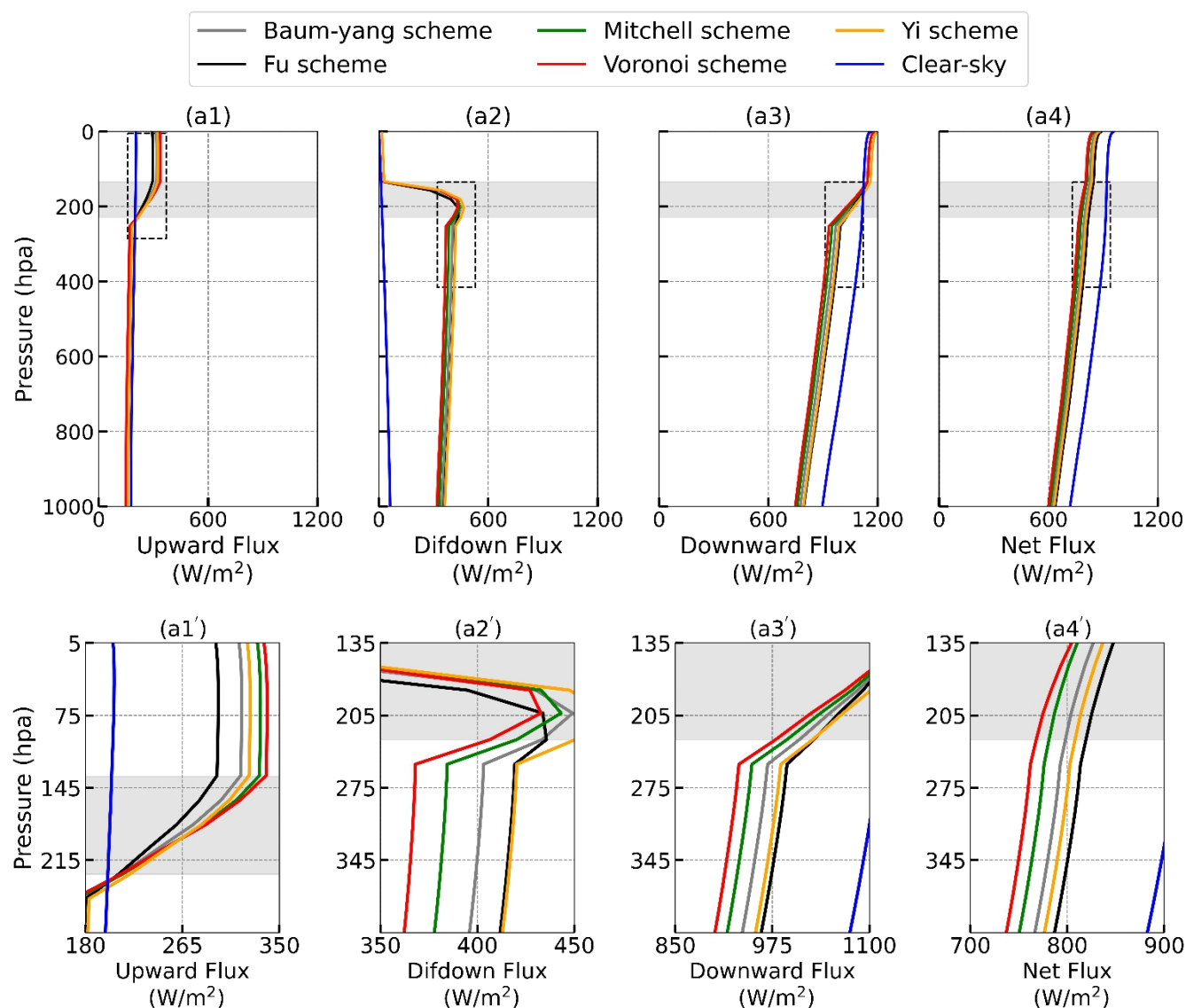
Figure 5. Shortwave radiative flux profiles (a1: upward flux; a2: diffuse downward flux; a3: downward flux; a4: net flux) of the Baum-yang scheme (black line), Voronoi scheme (red line), Mitchell scheme (green line), Yi scheme (yellow line), Fu scheme (black line) and clear conditions (blue line) for high tropical cirrus clouds, which are prescribed between 125.1 and 245.5 hPa, with ice particle effective diameters fixed at 45 μm and ice water paths fixed at 60 g m^{-2}. , for solar zenith angles at 60°. Graphics in black dotted box are magnified and displayed in (a1'-a4').
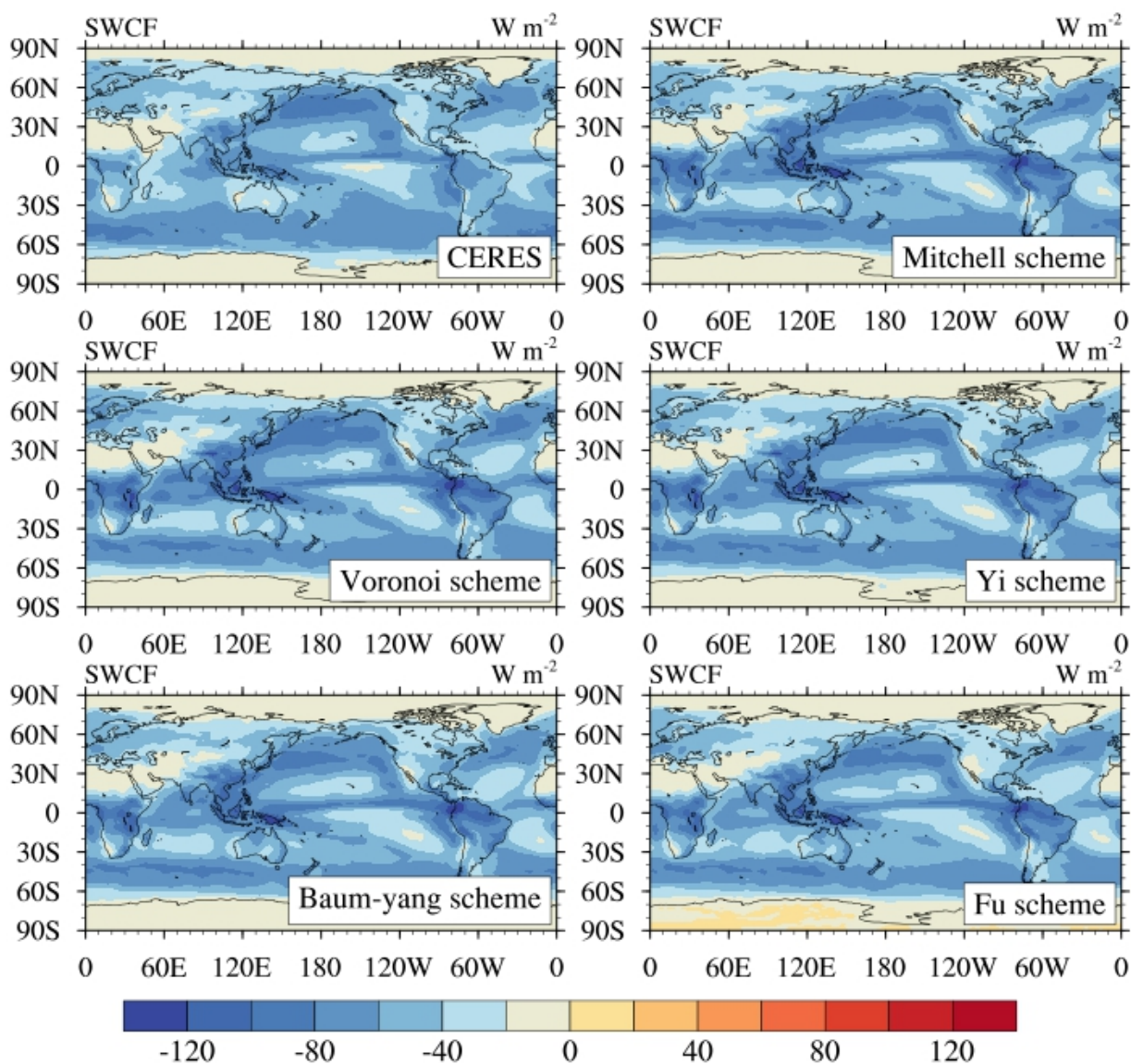
Figure 6. 10-yr average of TOA SWCF CAM5 simulations of Voronoi scheme, Mitchell scheme, Yi scheme, Baum-yang scheme and Fu scheme, and the validation data is 10-yr average CERES satellite data.
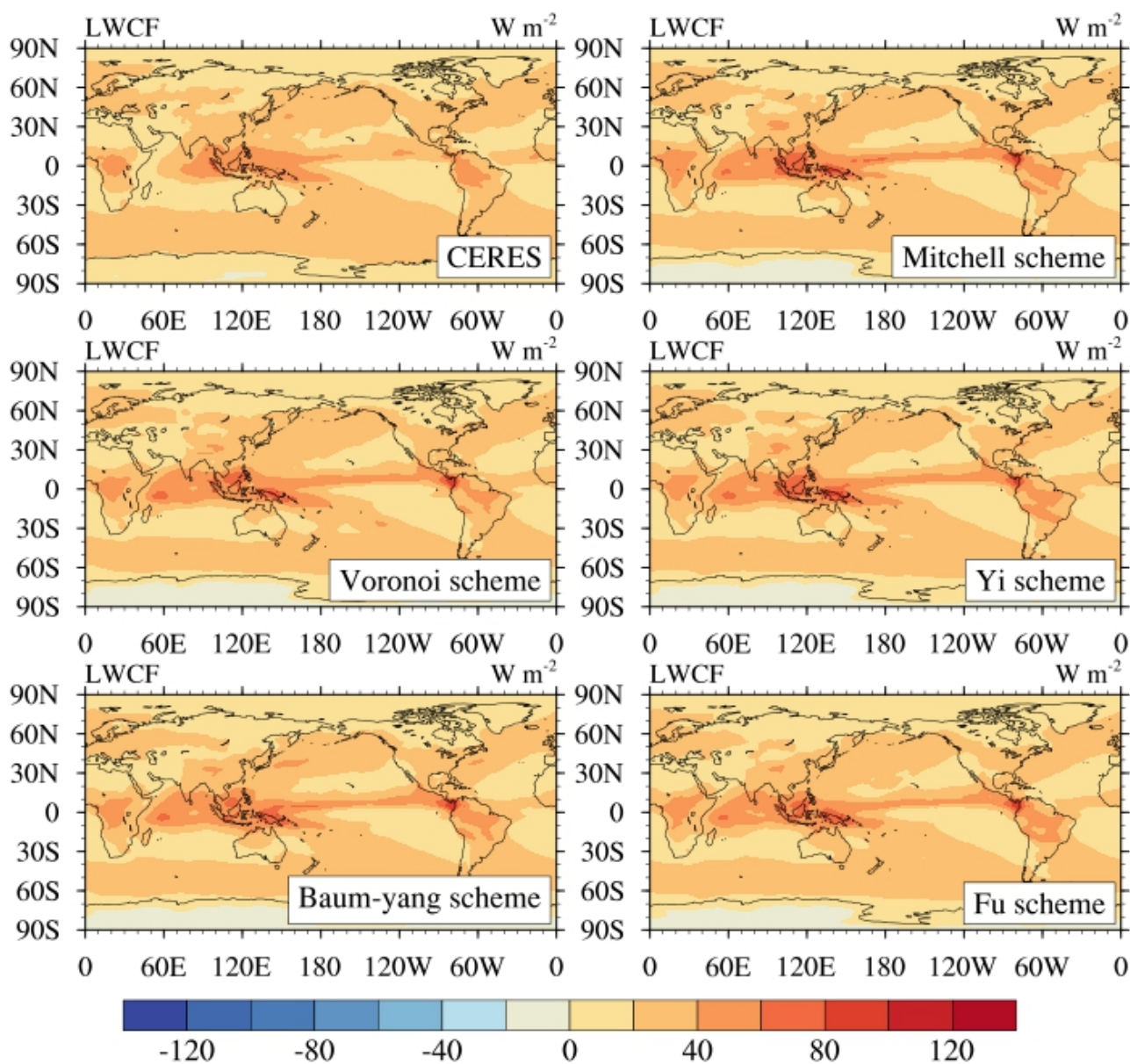
Figure 7. Same as the Fig. 9, but for 10-yr simulations of TOA LWCF.

610
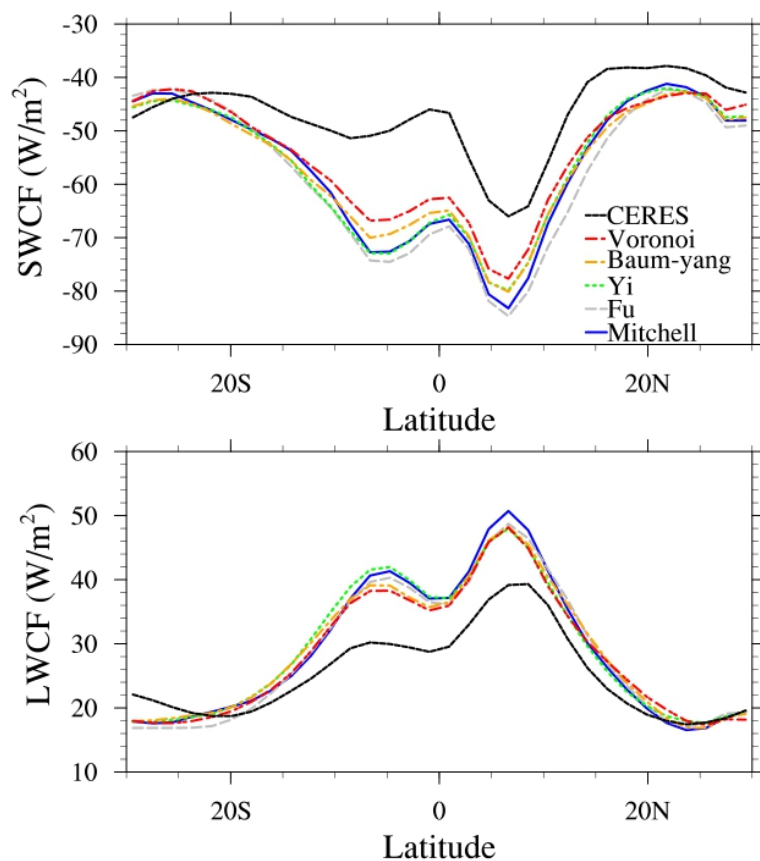
Figure 8. Zonal distributions patterns from 30°N to 30°S latitude of 10-yr annual mean simulations of TOA SWCF and LWCF for the Voronoi, Mitchell, Yi, Baum-yang and Fu scheme, validated by CERES satellite data, respectively.
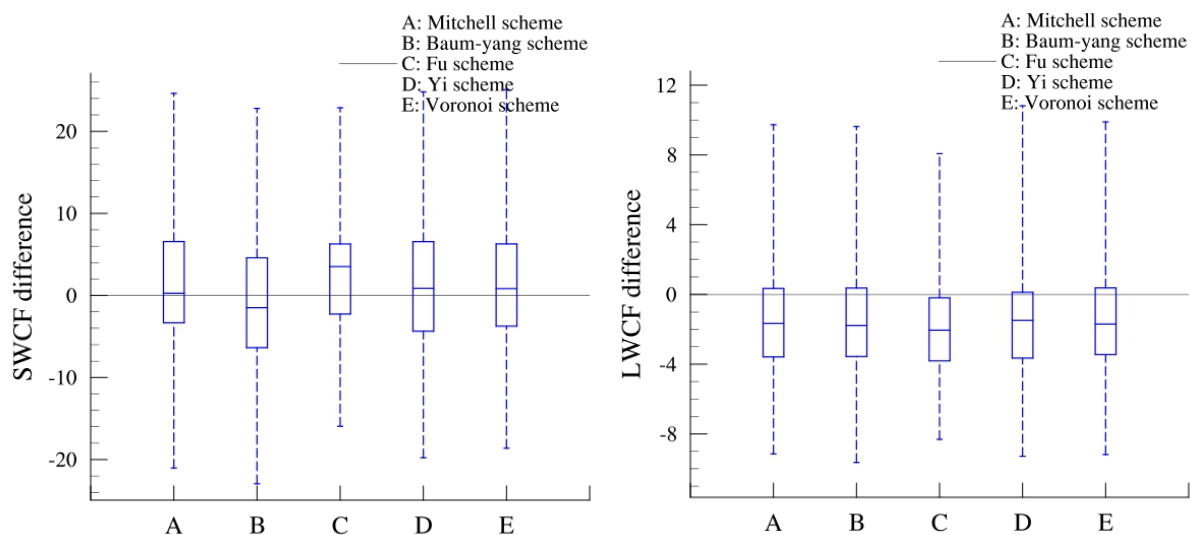
Figure 9. Box analysis of Zonal distributions of 10-yr annual mean SWCF (left) and LWCF (right) difference between the Mitchell, Voronoi, Fu, Baum-yang and Yi scheme, respectively.

630

635

640